Atmos. Meas. Tech. Discuss., 4, 1465–1492, 2011
www.atmos-meas-tech-discuss.net/4/1465/2011/
doi:10.5194/amtd-4-1465-2011

Atmospheric Measurement Techniques Discussions

Identification and localization of layers in the ionosphere using the eikonal and amplitude of radio occultation signals

A. G. Pavelyev[1], K. Zhang[2], J. Wickert[3], T. Schmidt[3], Y.-A. Liou[4], V. N. Gubenko[1], A. A. Pavelyev[1], R. R. Salimzjanov[1], and Y. Kuleshov[2]

[1]Kotelnikov Institute of Radio Engineering and Electronics of the Russian Academy of Sciences, Fryazino, Moscow region, Russia
[2]RMIT University School of Mathematical & Geospatial Sciences, GPO Box 2476V Melbourne 3001, Australia
[3]GeoForschungsZentrum Potsdam (GFZ-Potsdam), Telegrafenberg, 14473 Potsdam, Germany
[4]Center for Space and Remote Sensing Research, National Central University, Chung-Li, 320, Taiwan

Received: 19 January 2011 – Accepted: 3 February 2011 – Published: 1 March 2011

Correspondence to: A. G. Pavelyev (alxndr38@mail.ru)

Published by Copernicus Publications on behalf of the European Geosciences Union.

Abstract

Conditions for communication, navigation, and remote sensing in the ionosphere and atmosphere depend strongly on the ionospheric impact on the radio waves propagation. By use of the CHAllenge Minisatellite Payload (CHAMP) radio occultation (RO) data a description of different types of the ionospheric contributions to the RO signals at the altitudes 30–90 km of the RO ray perigee is introduced and compared with results of measurements obtained earlier in the communication link satellite-to-Earth at frequency 1.5415 GHz. An analytical model is introduced for description of the radio waves propagation in a stratified medium consisting of sectors having the spherically symmetric distributions of refractivity. Model presents analytical expressions for the phase path and refractive attenuation of radio waves. Model is applied for analysis of the radio waves propagation effects along a prolonged path including the atmosphere and two parts of the ionosphere. Model explains significant amplitude and phase variations at the altitudes 30–90 km of the RO ray perigee as connected with influence of the inclined ionospheric layers. An innovative eikonal acceleration technique is described and applied for the identification of the inclined ionospheric layers contributions and their location. Possibility to separate the influence of layered structures from contributions of irregularities and turbulence is analyzed.

1 Introduction

The high-stability radio signals transmitted at two GPS frequencies $f_1 = 1575.42$ MHz and $f_2 = 1227.60$ MHz from a GPS satellite and received at a GPS receiver aboard a low earth orbit (LEO) small/micro satellite are used for the radio occultation (RO) investigations (Melbourne et al., 1994; Ware et al., 1996; Kursinki et al., 1997; Hajj and Romans, 1998; Steiner et al., 1999; Wickert et al., 2001; Yakovlev, 2003; Jensen et al., 2003). When applied to ionospheric investigations RO method may be considered as a global tool and can be compared with the global earth- and space-based

AMTD
4, 1465–1492, 2011

radio tomography (e.g., Jakowski et al., 2004; Kunitsyn and Tereschenko, 2003 and references therein). RO measurements in the atmosphere can be impacted by ionospheric contributions because RO signal propagates through two different parts of the ionosphere. Usually the ionospheric influence may be described as a relatively slow change in the phase path excess without noticeable variations in the amplitude of RO signal. This change can be excluded by different methods of ionospheric correction (Melbourne et al., 1994; Vorob'ev and Krasilnikova, 1994; Gorbunov, 2002). Disturbed ionosphere significantly changes not only the phase but also the amplitude of the RO signals. Phenomenon of strong amplitude and phase frequency dependent variations in RO signals is often observed within the altitudes of the RO ray perigee h(T) between 40 and 90 km above the main part of the neutral atmosphere and below the E-layer of the ionosphere. The amplitude of RO signal presents new potential and capability for the research of the ionosphere (Sokolovskiy, 2000, 2002; Igarashi et al., 2000, 2001; Pavelyev et al., 2002, 2004, 2007, 2008a, b, 2009, 2010a; Liou et al., 2002, 2003, 2005, 2007; Liou and Pavelyev, 2006). The goal of this paper is (i) to introduce the description of different kinds of the ionospheric influence on the GPS RO signals within the altitudes of h(T) between 40 and 90 km, (ii) to present an analytical model for the refractive attenuation and phase path (eikonal) excess of electromagnetic waves in locally spherical symmetric media, and (iii) to demonstrate the possibility to identify contributions and to measure parameters of the inclined plasma layers by means of analyzing the CHAMP RO experimental data. The paper is structured as follows. In Sect. 2 the description of different kinds of the ionospheric impact on CHAMP RO signal is presented. Section 3 introduces an analytical model of the wave propagation through the ionosphere and atmosphere of the Earth. In Sect. 4 an example of ionospheric layers identification and the electron density retrieval is considered. Conclusions are given in Sect. 5.

AMTD
4, 1465–1492, 2011

2 Types of ionospheric influence on CHAMP RO signal

During a RO event the radio ray linking a LEO GPS receiver to a GPS satellite transmitter (marked by points L and G in Fig. 1, respectively) immerses gradually into the ionosphere and atmosphere. The LEO receiver measures the GPS dual-frequency phase (eikonal) delays and amplitudes of RO signal for subsequent retrieval of the vertical profiles of physical parameters in the ionosphere and atmosphere. In the case of absence of multipath propagation the RO inversion technique is based on two implicit assumptions: (i) the tangent point T, where the refractivity gradient is perpendicular to the RO ray, locates in the RO ray perigee (Fig. 1), and (ii) there is only one tangent point on the RO ray trajectory GTL. Under these assumptions, despite a prolonged path GTL, a relatively small area with a center at point T introduces the main contribution to the amplitude and phase variations of the RO signals (Igarashi et al., 2000, 2001). In this case the amplitude and phase variations of the RO signals are functions of the ray perigee height h(T) (Fig. 1) and the satellites' positions and velocities. Previously, the RO technology has been based mainly on analyzing the phase of the electromagnetic wave after propagating through the ionosphere and atmosphere (Ware et al., 1996). High sensitivity of the amplitude variations to ionospheric plasma layers can be used for description of different kinds of the ionospheric influence on RO signals in the trans-ionospheric communication links. Amplitude data can be used to obtain the vertical gradients of the electron density in the ionosphere and refractivity in the atmosphere independently (Pavelyev et al., 2002; Liou et al., 2002; Sokolovskiy, 2000, 2002).

The RO experiment aboard CHAMP was activated on 11 February 2001 (Wickert et al., 2001). Occultation measurements of the ionosphere and neutral atmosphere are scheduled autonomously by the BlackJack receiver instrument. Carrier phase path excesses (eikonals) at two frequencies f_1, f_2, and signal-to-noise ratio (SNR) at frequency f_1 are recorded at a sampling rate of 50 Hz. In the case of CHAMP RO experiments quiet ionospheric conditions have come to light in the form of small values of the S_4

AMTD
4, 1465–1492, 2011

index of the amplitude scintillations averaged at the altitudes H in the 40–90 km interval:

$$S_4 = [< (I(t) - < I >)^2 > / < I >^2]^{1/2} \quad (1)$$

where I and $< I >$ are the current and averaged intensities of the RO signals relevant to the propagation in the medium and in the open space. An example of quiet ionospheric conditions observed during the CHAMP RO experiments is shown in Fig. 2 (left panel). The amplitude curve 1 has low variations with index $S_4 = 1.7\%$. The phase path (eikonal) excesses $\Phi_1(t)$ and $\Phi_2(t)$ at f_1, and f_2 are shown by curves 2 and 3, respectively. Curve 4 corresponds to the combined eikonal $\Phi(t)$ from the following ionospheric correction formula (Melbourne et al., 1994):

$$\Phi(t) = [f_1^2 \Phi_1(t) - f_2^2 \Phi_2(t)]/(f_1^2 - f_2^2) \quad (2)$$

Examples of significant variations of the phase and amplitude of the GPS RO signals are given below in the altitude intervals of the ray perigee 40–90 km. These examples support suggestion that there exist the inclined ionospheric layers located along the RO ray trajectory. According to Fig. 1, the displacement d, correction to the height of the ionospheric layer Δh and its inclination δ with respect to the local horizontal direction are connected (Wickert et al., 2004) via equations:

$$\delta = d/a, \Delta h = 0.5 d\delta, \; d = (2\Delta h\, a)^{1/2} \quad (3)$$

where a is the Earth's radius (Fig. 1).

The isolated quasi-regular event with the influence of sporadic E-layers is shown in Fig. 2 (right panel). The fine structures corresponding to inclined sporadic E-layers are seen in the height h(T) intervals of 45–70 km. These phase and amplitude vertical distributions can correspond to the inclined sporadic E-layers usually located at the height about 93–103 km in the evening ionosphere. One can estimate the displacement of the ionospheric tangent point using Eq. (3). For $\Delta h = h' - h \approx 50$ km, one can obtain $\delta \approx 6^\circ$ and $d \approx (2\Delta h\, a)^{1/2} \approx 700$ km. These values can correspond to a sporadic E-layer at the altitude of 98 km declined by 6° relative to the horizontal direction and

AMTD
4, 1465–1492, 2011

located at the distance of 700 km away from the RO ray perigee. An example of the event with high quasi-regular variations in the amplitude and eikonal of the CHAMP RO signal with magnitude of the index $S_4 = 17\%$ is shown in Fig. 3. The eikonals at two frequencies change in the interval $2 \le \Phi_{1,2} \le 10$ m. These variations may be associated with layers in the electron density distribution. Strong ionospheric influence with diffraction structures in the RO signals is demonstrated in Fig. 4 (right) at the heights 98–105 km. This case can be considered as a consequence of diffraction of electromagnetic waves on sharp gradients of the electron density in a sporadic E-layer. Example of a noisy CHAMP event with high amplitude variations ($S_4 = 0.18$) is shown in Fig. 5. This event can be classified as a typical case, relevant to a noisy ionospheric contribution caused by intense ionospheric irregularities in the equatorial region in the midnight at 02:00 h Local Time (LT). The main part of the amplitude variations is limited to the interval $0.2 \le A \le 1.3$. The combined eikonal variations $\Phi(t)$ are also high that indicates sharp changes in the TEC which may possibly correspond to bubbles moving in the disturbed region of the ionosphere.

According to the analysis of CHAMP RO amplitude and phase data, five types of ionospheric influence on the RO signals can be established at the RO ray perigee altitudes between 40 km and 90 km:

- Quiet events (type 1, Fig. 2, left).
- Isolated quasi-regular flashes in the amplitude and phase of RO signal (type 2, Fig. 2, right).
- Regular events with quasi-periodical contributions to the amplitude of RO signal (type 3, Fig. 3).
- Diffractive events with diffraction phenomena in the ionosphere (type 4, Fig. 4)
- Noisy events with highly incoherent contribution of the ionospheric disturbance to the amplitude of RO signal (type 5, Fig. 5).

AMTD
4, 1465–1492, 2011

These types can be compared with the results obtained earlier by Karasawa et al. (1985) who investigated the temporal characteristics of the signals from a MARISAT satellite over the Indian Ocean at an elevation angle of 17.3° using a long term (16 months) measurements. Both C- and S-types of the ionospheric amplitude scintillations of radio signals are identified. The C-type is similar to noisy variations without any significant regular or periodical structure in the amplitude changes of the trans-ionospheric signals. The S-type consists of quasi-regular structures which can be associated with the influence of the bubbles or other types of disturbances in the ionospheric plasma. This coincidence in the types of CHAMP RO amplitude scintillations and the amplitude variations observed in the Earth-based experiments indicates common ionospheric mechanisms of their origin.

3 Analytical model for the phase path excess and refractive attenuation of RO signals

Effects of large-scale horizontal gradients on RO measurements have been considered by Ahmad and Tyler (1999). In this paper we describe analytical relationships for the phase path excess (eikonal) and refractive attenuation appropriate for the trans-ionospheric communication links satellite-to-satellite. One can assume a local spherical symmetry of the electron density distributions along the ray trajectory in the entrance and exit parts of the ionosphere. These parts of the ionosphere may have different centers of spherical symmetry (e.g., point O' in Fig. 1). The amplitude and phase variations of RO signals in this case may be investigated using an analytical model. The analysis of RO signal variations can then be used to find the distribution of the electron density and to estimate the location of the inclined layers in the ionosphere according to method described by Liou and Pavelyev (2006) and Pavelyev et al. (2009).

In Fig. 6 are shown three centers of local spherical symmetry associated with a single RO ray path in the ionosphere and atmosphere. They are located at different points O_1, O_2, and O_3 corresponding to three parts of the ray trajectory $G_1B_1B_2L$ in three

AMTD
4, 1465–1492, 2011

spherical sectors having boundaries at points B_1 and B_2, respectively: G_1B_1 (the ionosphere between transmitter G_1 and atmosphere), B_1B_2 (atmospheric part), and B_2L (the ionosphere between the receiver and atmosphere). Points G_1, L, O_1, O_2, and O_3 are assumed to be in the plane $G_1B_1B_2L$. This assumption corresponds to experimental RO data indicating a significant refraction effect in the plane of propagation. The central angles $\theta_1, \theta_2, \theta_3$ between directions to transmitter G_1 and receiver L have vertices located at points O_1, O_2, O_3 (Fig. 6). The distances G_1O_1, G_1O_2, G_1O_3 and LO_1, LO_2, LO_3 are equal to D_1, D_2, D_3, and R_1 (L), R_2 (L), R_3 (L), respectively. Points G_2, G_3 (actually G_2 and G_3 are apparent radio images of transmitter G_1 as seen from points B_1 and B_2) are intersections of the tangents to the RO ray trajectory $G_1B_1B_2L$ at the points B_1, B_2 with the straight lines O_1G_1 and O_2G_2, respectively. The angles μ_1, μ_2 and μ_3, μ_4 have common vertices at the points G_2 and G_3. Variables μ_1, μ_2 are the angles between the tangent to the ray trajectory $G_1B_1B_2L$ at point B_1 and directions of O_1G_2, O_2G_2, respectively (Fig. 6). Variables μ_3, μ_4 are the angles between the straight line G_3B_2 – the tangent to the ray trajectory $G_1B_1B_2L$ at point B_2 and directions O_2G_3, O_3G_3, accordingly (Fig. 6). Dependence of the phase path excess (eikonal) and refractive attenuation on the impact parameter p may be considered separately for three parts of RO ray trajectory $G_1B_1B_2L$. In the general case of N spherical symmetric sectors the eikonal Φ corresponding to the ray $G_1B_1B_2L$ (Fig. 6) is a sum (Pavelyev et al., 2010b):

$$\Phi = \sqrt{D_1^2 - p_1^2} + \sqrt{R_N^2 - p_N^2} + \sum_{i=1}^{i=N-1} b_i \cos(\gamma_i - \xi_i - \alpha_i) + \sum_{m=1}^{N} [p_m \xi_m(p_m) + \kappa_m(p_m)] \quad (4)$$

where p_i, ξ_i (p_i),κ_i (p_i) are the impact parameter, the bending angle, and the main refractivity part of the phase path corresponding to the i-th spherical sector. Owing to the condition of spherical symmetry the impact parameters $p_1, p_2, \ldots, p_N$ satisfy to the following relationships which are valid inside the i-th spherical sector:

$$p_i = n(R_i) R_i \sin \gamma_e, i = 1, \ldots, N \quad (5)$$

AMTD
4, 1465–1492, 2011

where $n(R_i)$ is the refractive index, γ_e is the angle between the tangent to the ray trajectory G_1L at the current point E and direction to the center of spherical sector. The tangents to the ray trajectory G_1L and the directions to the centers O_1, O_2, O_3 make the angles γ_1, γ_2, γ_3 at the point G_1 and β_1, β_2, β_3 at the point L, respectively (Fig. 6). Relationships between the impacts p_1, p_2, p_3, central angles θ_1, θ_2, θ_3 and bending angles ξ_1, ξ_2, ξ_3 can be obtained using the geometry of the ray path $G_1B_1B_2L$ shown in Fig. 6:

$$p_2 = p_1 + b_1 \sin(\gamma_1 - \xi_1 - \alpha_1);\ p_3 = p_2 + b_2 \sin(\gamma_2 - \xi_1 - \xi_2 - \alpha_2) \quad (6)$$

$$\theta_i = \pi + \xi(p_1) - \gamma_i - \beta_i, \xi(p_1) = \xi_1(p_1) + \xi_2(p_2) + \xi_3(p_3);\quad i = 1, 2, 3 \quad (7)$$

A method introduced previously (Pavelyev and Kucherjavenkov, 1978) to the case of a spherical symmetric medium is used by Pavelyev et al. (2010b) in the geometric optics approximation for general case of a medium consisting of N spherical symmetric sectors to obtain an exact expression for the refractive attenuation of electromagnetic waves X_L:

$$X_L = R_0^2 \sin\gamma_1 / [d R_i(L) \cos\beta_i \left|\partial\theta_i / \partial\gamma_1\right| dS(1)\ldots S(N-1)],\quad i = 1,\ldots,N;$$
$$S(i) = \sin\mu_{2i-1} / \sin\mu_{2i}, S(0) = 1, d = R_N(L)\sin\Theta \quad (8)$$

Relationships (4)–(8) present the main content of the analytical model in the partial case of three spherical sectors. In the plane $G_1B_1B_2L$ the phase path and the refractive attenuation depend, respectively, on the sum of the phase changes and the bending angles in the spherical sectors and practically do not depend on locations of their boundaries. The effects of a spherical symmetric layer do not depend significantly on its location in the first, second or third spherical sectors. Any intense locally spherical symmetric layer along the ray $G_1B_1B_2L$ in the ionosphere may produce the unexpected strong variations in the amplitude and phase of the RO signals at the 40–90 km altitudes of the RO ray perigee since values of the impact parameters in an inclined ionospheric and atmospheric layer are different. Therefore displacement of

AMTD
4, 1465–1492, 2011

the tangent point is a main cause of systematic error in the RO estimation of the altitude of inclined ionospheric layers. This conclusion may be valid also in the case of electromagnetic waves propagation in the satellite-to-Earth communication links.

The developed analytical model allows ray tracing of the RO signals. If the impact parameter p_1 is known then one can consequently determine the impact parameters p_i, $i = 2,\ldots,N$ and the refraction angle $\xi(p_1)$ from Eq. (6 and 7) and then recalculate the phase path $\Phi(p_1)$ and the refractive attenuation X_L from Eqs. (4) and (8). Note the important feature of the introduced model. If in the k-th sector the refraction effect is absent, then the dimension N of model can be lowered to $N-1$. In this case the next equalities are valid:

$$\mu_{2k-1} = \mu_{2k}; \quad S(k) = 1 \tag{9}$$

and the refractive attenuation Eq. (8) does not depend on the contribution from the k-th spherical sector.

The phase path of electromagnetic waves after propagating through the ionosphere and atmosphere may be considered according to relationship (4) as a linear function of the bending angles in the corresponding sectors if the refraction effect is small. Therefore the linear methods of ionospheric correction introduced earlier (Melbourne et al., 1994; Vorob'ev and Krasilnikova, 1994) should be effective in the case of propagation through several spherical symmetric sectors in the case of undisturbed ionosphere. However the amplitude of RO signal is a nonlinear function of the bending angle and in the case of the disturbed ionosphere it is a subject for strong perturbations.

Let us consider the partial case when the refraction effect exists in the first sector according to the ionospheric influence and is absent in the remaining sectors. This case is typical for the amplitude and phase variations at the altitudes 40–90 km where the neutral atmosphere's influence is minimal. In this case the points G_2, G_3, ...,G_N are coinciding. As a consequence, the next relationship is fulfilled:

$$\mu_3 = \mu_2, \mu_5 = \mu_4, \ldots, \mu_{2N-3} = \mu_{2N-4} \tag{10}$$

AMTD
4, 1465–1492, 2011

After substitution of Eq. (10) in the relationship (8) one can obtain:

$$X_L = R_0^2 \sin\gamma_1 / [R_1^2 (L) \cos\beta_1 |\partial\theta_1 / \partial\gamma_1| \sin\theta_1 (L)] \quad (11)$$

Equation (11) has been obtained previously (Pavelyev and Kucherjavenkov, 1978). If the tangent point exists in the first sector, and there is a sharp gradient of refractivity, then one can observe in this case strong variations of the amplitude and phase of the RO signals at the low altitudes of RO rays perigee h 40–90 km because of a significant displacement of the centre O_1. However according to spherical symmetry one may estimate the electron density distribution in inclined ionospheric plasma layers by using the Abel transformation.

As follows from the introduced model the ionospheric contribution in the RO signals can be significant at different altitudes of the RO ray perigee in 40–90 km interval if the following two necessary and sufficient conditions are fulfilled: (i) the ionospheric part of the RO signals path contains a tangent point; and (ii) there is a refractivity layer with sharp gradient perpendicular to the ray $G_1B_1B_2L$ in the vicinity of the tangent point. In the simplest case, when an inclined plasma layer exists only on one part of the ray $G_1B_1B_2L$ and the influence of the neutral atmosphere is weak, the analytical model predicts the displacement of the tangent point from the ray perigee T to a plasma layer. As a result one may observe unusually strong amplitude and phase variations of the RO signals in the 40–90 km interval of the RO ray perigee height h(T).

4 Identification and location of plasma layers

Liou and Pavelyev (2006), Pavelyev et al. (2007), Liou et al. (2007), and Pavelyev et al. (2009) detected and validated a connection between the phase excess $\Phi(p)$ (eikonal) acceleration and the refractive attenuation of electromagnetic waves $X(t)$:

$$1 - X(t) = m\,a = m\,d(\lambda F_d)/dt = m\,d^2\Phi(p)/dt^2;$$
$$m = q/(dp_s/dt)^2; \quad q = (R_0 - d_2)d_2/R_0 \quad (12)$$

AMTD
4, 1465–1492, 2011

Value m has dimension [$s^2\,m^{-1}$]. An inverse value $\frac{1}{m}$ may be considered as a module of the tangent point T centripetal acceleration oriented in the direction to point L. Equation (12) connects the refractive attenuation $X(t)$, derivative of the Doppler frequency F_d on time and the phase acceleration $a = d[\lambda F_d(t)]/dt = d^2\Phi(p)/dt^2$ via a relationship similar to classical dynamics equation. Variations of the refractive attenuation $1 - X(t)$ may be considered as a ratio of the eikonal acceleration and centripetal acceleration of point T. The impact parameter p_s and distances R_0 and d_2 are shown in Fig. 1. Parameters m and dp_s/dt may be evaluated from the orbital data. The distance d_2 can be evaluated from the relationship (Pavelyev et al., 2009):

$$d_2 = 2R_0\,\beta\,[1+2\beta\,(1-w/v) + (1-4\beta\,w/v)^{1/2}]^{-1},$$
$$\beta = mv^2/R_0, m = [1-X(t)]/a \tag{13}$$

where w and v are the velocity components of the GPS and LEO satellites, respectively, which are perpendicular to the straight line GL in the plane GOL (Fig. 1). Components w and v are positive when they oriented towards the direction to the point O and are negative in the opposite case. Analysis of the CHAMP GPS RO data provided by Pavelyev et al. (2008a, b) indicates correctness of the relationship (12) for the atmosphere and layered structures in the ionosphere. The relationship (12) broaden an applicable domain of the RO method. Equation (12) presents a possibility to convert the phase acceleration a and/or Doppler frequency F_d to the refractive attenuation X_p (Pavelyev et al., 2009, 2010a, b). From these derived refractive attenuation and amplitude data one can estimate the integral absorption of electromagnetic waves (Pavelyev et al., 2009). It is shown that there is a possibility to apply the developed technique for identification and location of sharp layered sporadic Es structures in the ionosphere (Pavelyev et al., 2010). This is important for study of the radio wave propagation effects in the atmospheric telecommunication links and for remote sensing of the atmosphere and ionosphere.

To consider the possibility to identify the plasma layers contribution in the RO signals we will use a CHAMP RO event 0117 (14 January 2001, 00:56 LT, 76.4° N, 172.7° W)

AMTD
4, 1465–1492, 2011

with strong quasi-regular amplitude and phase variations. The refractive attenuation of the CHAMP RO signals at the first GPS frequency f_1 (curve 1) and phase path excesses at the GPS frequencies f_1 and f_2 (curves 2 and 3) as functions of the RO ray perigee altitude h are shown in Fig. 7 (left panel). The curves 2 and 3 have been obtained after subtracting a regular phase trend connected with the upper ionosphere influence. The form of the refractive attenuation variations indicates the impact of the ionospheric disturbances in the 72–98 km interval of h. This disturbance consists of two patches which are responsible for the maximums in the intensity changes in the 72–78 km and 84–96 km intervals of h. In the 78–84 km interval of height h the intensity variations are notable. However they are not so strong. The phase changes at frequencies f_1 and f_2 in Fig. 7, (left panel), also indicate a two-layered structure at the altitudes 75 and 90 km. The eikonal accelerations at both frequencies f_1 and f_2 (curves 2 and 3 in Fig. 7, right panel) reveal the fine structures in the phase of RO signals. The eikonal acceleration a has been estimated numerically by double differentiation over a fixed time interval Δt. The value of Δt was equal to 0.42 s. The strongest variations of the eikonal acceleration are observed almost in the same altitude intervals as for the refractive attenuation. In this interval the eikonal acceleration and refractive attenuation variations are strongly connected and may be considered as coherent oscillations caused by layered structures. It is important that at altitudes of below 72 km and higher than 98 km the refractive attenuation variations are small and do not have any connection with changes of the eikonal acceleration (Fig. 7, right panel). This indicates different incoherent mechanism of the significant eikonal variations at the heights $h \leq 72$ km and $h \geq 98$ km. As a further identification step, further examination is conducted to locate the indicated layers in the ionosphere. If parameter m is estimated from the experimental data using Eq. (13), it is possible to find the new value of distance T'L $\approx d_2'$ and to determine the displacement of the new tangent point T' and the location of a layer relative to point T (Fig. 1):

AMTD
4, 1465–1492, 2011

$$d = d_2' - (R_2^2 - p_s^2)^{1/2} \quad (14)$$

The results of evaluation of the parameter m, displacement d, and the corrected layer altitude h are given in Table 1 as functions of the ray perigee altitude h(T). Data in Table 1 correspond to the CHAMP GPS RO event No. 0117. The variations of the refractive attenuations $X_p - 1$ and $X_a - 1$ calculated from the phase and amplitude data, and the estimated m values are shown in the second, third, and seventh columns in Table 1 as functions of the ray perigee height $H = h$(T) in the two intervals of 97.33–97.61 km Eq. (1); and 72.13–72.23 km Eq. (2). These intervals correspond to a maximum in the absolute values of the refractive attenuation and eikonal acceleration variations relevant to the curves 1 and 2 shown in Fig. 7 (right panel). The displacement d and the estimated value of the layers altitude h' are presented in the forth and fifth columns (Table 1) respectively. The displacement d changes between 140 km and 210 km in the interval (1), and 357 km–714 km in the interval (2). These values correspond to the displacement of the tangent point from the ray perigee in direction to point G. The corresponding corrections to the altitude H are about 2 km–6 km in the interval (1) and 20 km–30 km in the interval (2). This analysis indicates that the ionospheric layers are located in the entrance part of the ionosphere between point G and T (Fig. 1) at the distance d in the interval 300–500 km. The corresponding values Δh change in the 2–30 km interval. Identification of the sporadic Es layer justifies the application of the Abel' transform for solving the inverse problem. The resulting electron density distribution is shown in Fig. 8. Two patches of the ionospheric layer are clearly seen in Fig. 8. The first patch of the layers is located on line GT at a distance 300 km from point T (curves 1 and 2 in Fig. 8). It is concentrated in the 92–104 km interval with inclination to the horizontal direction δ of about 3°. The second patch (Fig. 8, curve 3 and 4) is located on the line GT in the 94–100 km interval at the distance 500 km relative to the tangent point T (Fig. 1) with inclination of about 5°. Between two patches the plasma density is small. The amplitude variations in the 70–96 km interval of altitude H are connected with sporadic E-layer located along the line GT in the altitude interval 92–104 km at the distance 300–500 km relative to point T. The inclination of the sporadic E-layer

AMTD
4, 1465–1492, 2011

changes along the line GT from 3° up to 5°. As follows from Fig. 8, the electron density variations are concentrated in the interval $0 < N(h) < 3.5 \times 10^{10}$ [electrons/m^{t3}]. These magnitudes of $N(h)$ are somewhat below the usual values of $N(h)$ for sporadic E-layers. The height interval of the amplitude variations is nearly equal to the height interval of the variations in the electron density and its gradient. Therefore the introduced method appears to have a considerable potential to resolve the uncertainty in the location of the inclined layer between the part GT and LT of the ray trajectory. Additional validation of this method through analyzing the CHAMP data and comparison with ground-based ionosonde information is the task for the future work.

5 Conclusions

A new analytical model is introduced to account for local mechanism of the multiple-RO ionospheric effects which incorporates horizontal gradients in the ionosphere. The model gives analytical expressions for the phase path excess, eikonal, and refractive attenuation of the electromagnetic waves propagating through the disturbed ionosphere. The introduced analytical model indicates a possibility for applications of the Abel transform for estimating the electron density distribution in the inclined ionospheric plasma layers. Analysis of CHAMP RO data and the analytical model have demonstrated the importance of comparative analysis of the amplitude and phase channels of the satellite radio-holograms for classifying ionospheric influence on RO signals. Preliminary analysis reveals five types of ionospheric impacts on the CHAMP RO signals at the altitudes of RO perigee 40–90 km: (i) quiet events; (ii) isolated quasi-regular flashes (possible contribution of the inclined sporadic E-layers); (iii) events with quasi-periodical changes of the amplitude and phase (possible source – wave structures in the electron density); (iv) diffractive events with a clearly identifiable diffraction pattern in the amplitude and phase; and (v) events with noisy contribution of the ionospheric disturbances to the amplitude. The noisy and quasi-regular amplitude variations in the RO signals correspond to the earlier described C- and S-type amplitude scintillations in

AMTD
4, 1465–1492, 2011

the trans-ionospheric satellite-to-Earth links. Analysis of the CHAMP RO data indicates a possibility of identification, location and evaluation of the electron density distribution and its gradient in the inclined ionospheric layers.

Acknowledgements. We are grateful to GFZ-Potsdam for access to the CHAMP RO data. This research is supported through an Australian Research Council project (ARC- LP0883288) and the Department of Industry, Innovation, Science and Research of Australia International Science Linkage projects (DIISR/ISL-CG130127). Work has been partly supported by National Science Council and National Space Organization of Taiwan, R.O.C., grants NSC 98-2111-M-008-012-MY3 and 98-NSPO(B)-IC-FA07-01(X), by grant No. 10-02-01015-a, Russian Fund of Basic Research, and by program OFN-15 of Russian Academy of Sciences.

References

Ahmad, B. and Tyler, L.: Systematic errors in atmospheric profiles obtained from Abelian inversion of radio occultation data: Effects of large-scale horizontal gradients, J. Geophys. Res., 104(D4), 3971–3992, 1999.

Gorbunov, M. E.: Ionospheric correction and statistical optimization of radio occultation data, Radio Sci., 37(8), 17-1–17-9, 2002.

Hajj, G. A. and Romans, L. J.: Ionospheric electron density profiles obtained with the Global Positioning System: Results from GPS/MET experiment, Radio Sci., 33(1), 175–190, 1998.

Hocke, K., Pavelyev, A., Yakovlev, O., Barthes, L., and Jakowski, N.: RO data analysis by radio holographic method, J. Atmos. Sol.-Terr. Phys., 61, 1169–1177, 1999.

Igarashi, K., Pavelyev, A. G., Hocke, K., Kucherjavenkov, A. I., Matugov, S. S., Yakovlev, O. I., Pavelyev, D., and Zakharov, A.: Radio holographic principle for observing natural processes in the atmosphere and retrieving meteorological parameters from radio occultation data, Earth Planet. Space, 52, 11, 868–875, 2000.

Igarashi, K., Pavelyev, A. G., Hocke, K., Pavelyev, D., and Wickert, J.: Observation of wave structures in the upper atmosphere by means of radio holographic analysis of the RO data, Adv. Space Res., 27(6–8), 1321–1327, 2001.

Jensen, A. S., Lohmann, M., Benzon, H.-H., and Nielsen, A. S.: Full spectrum inversion of radio occultation signals, Radio Sci., 38(3), 1040, doi:10.1029/2002RS002763, 2003.

AMTD
4, 1465–1492, 2011

Jakowski, N., Leitinger, R., and Angling, M.: Radio occultation techniques for probing the ionosphere, Ann. Geophys.-Italy, supplement to 47(2/3), 1049–1066, 2004.
Karasawa, Y., Yasukawa, K., and Yamada, M.: Ionospheric scintillation measurement at 1.5 GHz in mid-latitude region, Radio Sci., 20(3), 643–651, 1985.
Kunitsyn, V. E. and Tereshchenko, E. D.: Ionospheric Tomography, Springer-Verlag, Berlin, 2003.
Kursinski, E. R., Hajj, G. A., Schofield, J. T., Linfield, R. P., and Hardy, K. R.: Observing Earth's atmosphere with radio occultation measurements using the global positioning system, J. Geophys. Res., 102, 23429–23465, 1997.
Liou, Y.-A. and Pavelyev, A. G.: Simultaneous observations of radio wave phase and intensity variations for locating the plasma layers in the ionosphere, Geophys. Res. Lett., 33(10), L23102, doi:10.1029/2006GL027112, 2006.
Liou, Y.-A., Pavelyev, A. G., Huang, C.-Y., Igarashi, K., and Hocke, K.: Simultaneous observation of the vertical gradients of refractivity in the atmosphere and electron density in the lower ionosphere by radio occultation amplitude method, Geophys. Res. Lett., 29(21), 43-1–43-4, 2002.
Liou, Y.-A., Pavelyev, A. G., Huang, C.-Y., Igarashi, K., Hocke, K., and Yan, S. K.: Analytic method for observation of the GW using RO data, Geophys. Res. Lett., 30(23), ASC 1-1–1-5, 2003.
Liou, Y.-A., Pavelyev, A. G., Pavelyev, A. A., Wickert, J., and Schmidt, T.: Analysis of atmospheric and ionospheric structures using the GPS/MET and CHAMP radio occultation data base: A methodological review, GPS Solutions, 9(2), 122–143, 2005.
Liou, Y.-A., Pavelyev, A. G., Liu, S.-F., Pavelyev, A. A., Nick, Y., Huang, C.-Y., and Fong, C.-J.: FORMOSAT-3/COSMIC GPS Radio Occultation Mission: Preliminary Results, IEEE Transactions on Geoscience and Remote Sensing, 45(11), 3813–3826, 2007.
Melbourne, W. G.: Radio Occultations Using Earth Satellites: A Wave Theory Treatment, Jet Propulsion Laboratory California Institute of Technology, Monograph 6, Deep space communications and navigation series, Issued by the Deep Space Communications and Navigation Systems Center of Excellence Jet Propulsion Laboratory California Institute of Technology, edited by: Yuen, J. H., 610 pp., 2004.
Melbourne, W. G., Davis, E. S., Duncan, C. B., Hajj, G. A., Hardy, K. R., Kursinski, E. R., Meehan, T. K., Young, L. E., and Yunck, T. P.: The Application of Spaceborne GPS to Atmospheric Limb Sounding and Global Change Monitoring, JPL Publication, 94(18), 147 pp.,

AMTD
4, 1465–1492, 2011

1994.
Pavelyev, A. G. and Kucherjavenkov, A. I.: Refractive attenuation in the planetary atmospheres, Radio Eng. Electron. Phys., 23(10), 13–19, 1978.
Pavelyev, A. G., Liou, Y.-A., Huang, C. Y., Reigber, C., Wickert, J., Igarashi, K., and Hocke, K.: Radio holographic method for the study of the ionosphere, atmosphere and terrestrial surface using GPS occultation signals, GPS Solutions, 6, 101–108, 2002.
Pavelyev, A. G., Liou, Y. A., and Wickert, J.: Diffractive vector and scalar integrals for bistatic radio- holographic remote sensing, Radio Sci., 39(7), RS4011, doi:10.1029/2003RS002935, 2004.
Pavelyev, A. G., Liou, Y. A., Wickert, J., Schmidt, T., Pavelyev, A. A., and Liu, S. F.: Effects of the ionosphere and solar activity on radio occultation signals, Application to CHAllenging Minisatellite Payload satellite observations, J. Geophys. Res., 112, A06326, doi:10.1029/2006JA011625, 2007.
Pavelyev, A. G., Wickert, J., and Liou, Y.-A.: Localization of plasma layers in the ionosphere based on observing variations in the amplitude and phase of radiowaves along the satellite-to-satellite path, Radiophys. Quantum El., 51(1), 1–8, 2008a.
Pavelyev, A. G., Liou, Y.-A., Wickert, J., Pavelyev, A. A., Schmidt, T., Igarashi, K., and Matyugov, S. S.: Location of layered structures in the ionosphere and atmosphere by use of GPS occultation data, Adv. Space Res., 42, 224–228, 2008b.
Pavelyev, A. G., Liou Y. A., Wickert J., Gavrik A. L., and Lee, C. C.: Eikonal acceleration technique for studying of the Earth and planetary atmospheres by radio occultation method, Geophys. Res. Lett., 36, L21807, doi:10.1029/2009GL040979, 2009.
Pavelyev, A. G., Liou, Y.-A., Wickert, J., Schmidt, T., Pavelyev, A. A., and Matyugov, S. S.: Phase acceleration: a new important parameter in GPS occultation technology, GPS Solutions, 14(1), 3–14, doi:10.1007/s10291-009-0128-1, 2010a.
Pavelyev, A. G., Liou, Y. A., Wickert, J., Zhang, K., Wang, C.-S., and Kuleshov, Y.: Analytical model of electromagnetic waves propagation and location of inclined plasma layers using occultation data, Pr. Electromagn. Res. S., 106, 177–202, doi:10.2528/PIER10042707, 2010b.
Sokolovskiy, S. V.: Inversion of RO amplitude data, Radio Sci., 35(1), 97–105, 2000.
Sokolovskiy, S. V., Schreiner, W., Rocken, C., and Hunt, D.: Detection of high-altitude ionospheric irregularities with GPS/MET, Geophys. Res. Lett., 29(3), 621–625, 2002.
Steiner, A. K. and Kirchengast, G.: GW spectra from GPS/MET occultation observations, J. Atmos. Ocean. Tech., 17, 495–503, 2000.

AMTD
4, 1465–1492, 2011

Steiner, A. K., Kirchengast, G., and Ladreiter, H. P.: Inversion, error analysis, and validation of GPS/MET occultation data, Ann. Geophys., 17, 122–138, doi:10.1007/s00585-999-0122-5, 1999.

Vorob'ev, V. V. and Krasilnikova, T. G.: Estimation of accuracy of the atmosphere refractive index recovery from Doppler shift measurements at frequencies used in the NAVSTAR system, Izv. Russ. Acad. Sci., Physics of the Atmosphere and Ocean, Engl. Transl., 29(10), 602–609, 1994.

Vorob'ev, V. V., Gurvich, A. S., Kan, V., Sokolovskiy, S. V., Fedorova, O. V., and Shmakov, A. V.: Structure of the Ionosphere from the Radio-Occultation GPS-"Microlab-1" Satellite Data: Preliminary Results, Earth. Obs. Remot. Sen.+, 15, 609–622, 1999.

Ware, R., Exner, M., Feng, D., Gorbunov, M., Hardy, K., Herman, B., Kuo, Y.-H., Meehan, T., Melbourn, W., Rocken, C., Schreiner, W., Sokolovskiy, S., Solheim, F., Zou, X., Anthes, R., Businger, S., and Trenberth, K.: GPS soundings of the atmosphere from low earth orbit: Preliminary results, Bull. Am. Meteor. Soc., 77, 19–40, 1996.

Wickert, J., Reigber, C., Beyerle, G., Konig, R., Marquardt, C., Schmidt, T., Grunwaldt, L., Galas, R., Meehan, T. K., Melbourne, W. G., and Hocke, K.: Atmosphere sounding by GPS radio occultation: First results from CHAMP, Geophys. Res. Lett., 28(19), 3263–3266, 2001.

Wickert, J., Pavelyev, A. G., Liou, Y. A., Schmidt, T., Reigber, C., Igarashi, K., Pavelyev, A. A., and Matyugov, S.: Amplitude scintillations in GPS signals as a possible indicator of ionospheric structures, Geophys. Res. Lett., 31(24), L24801, doi:10.1029/2004GL020607, 2004.

Yakovlev, O. I.: Space Radio Science, Taylor and Francis, London, 306 pp., 2003.

Yeh, K. C. and Liu, C. H.: Radio wave scintillations in the ionosphere, Proc. IEEE, 70(7), 324–360, 1982.

AMTD
4, 1465–1492, 2011

Table 1. Location of ionospheric layers.

H	$X_p - 1$	$X_a - 1$	d, km	h, km	$\delta°$	m, $s^2\ m^{-1}$
97.61	0.06429	0.07053	140.74	99.163	1.26	0.87587
97.58	0.06584	0.07291	155.00	99.461	1.38	0.88391
97.55	0.06694	0.07458	164.73	99.673	1.47	0.88940
97.52	0.06633	0.07550	198.30	100.59	1.77	0.90861
97.49	0.06610	0.07563	206.26	100.81	1.84	0.91316
97.46	0.06481	0.07478	219.46	101.22	1.96	0.92078
97.42	0.06299	0.07309	228.50	101.50	2.04	0.92599
97.39	0.06081	0.07047	226.61	101.41	2.02	0.92484
97.36	0.05814	0.06694	216.38	101.02	1.93	0.91883
97.33	0.05460	0.06265	210.95	100.81	1.88	0.91563
72.23	0.04132	0.06316	714.35	112.09	6.39	1.17436
72.19	0.04029	0.05866	626.54	102.86	5.60	1.11844
72.16	0.03934	0.05328	498.98	91.618	4.46	1.04047
72.13	0.03786	0.04721	357.26	82.105	3.19	0.95806

AMTD
4, 1465–1492, 2011

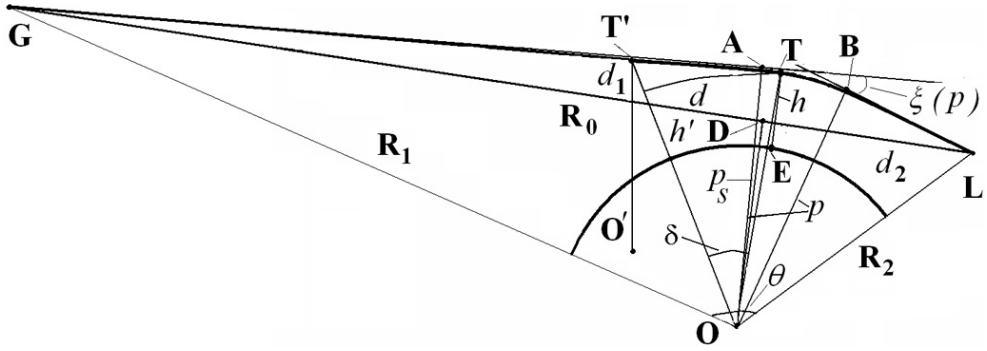

Fig. 1. Geometry of radio ray path in RO experiment.

AMTD
4, 1465–1492, 2011

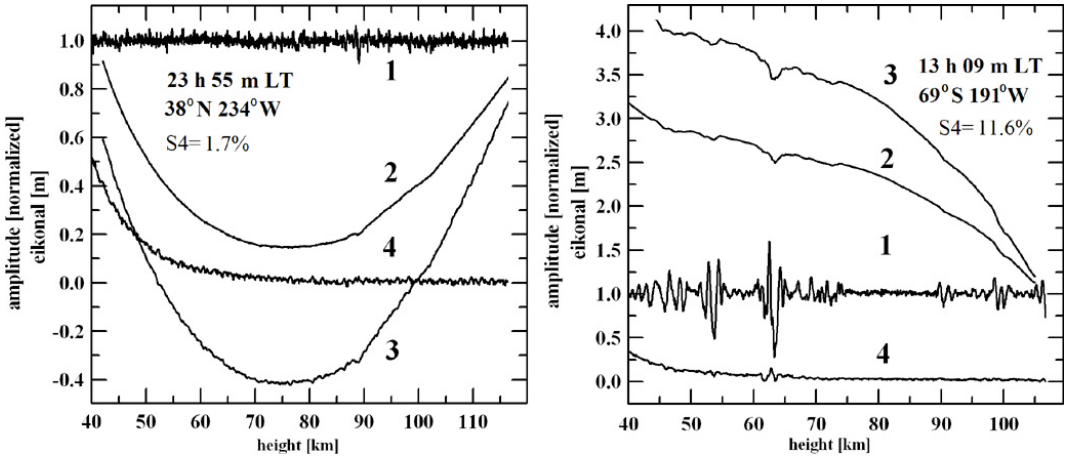

Fig. 2. Amplitude and phase measurements of the CHAMP RO signals in both quiet (left) and slightly disturbed (right) ionosphere (events No. 0174 and 0023, 24 February and 16 June 2003). Local time of the event and coordinates of the RO ray perigee T are shown in the graphs. The S_4 index value is shown in the lower line of the insert.

AMTD
4, 1465–1492, 2011

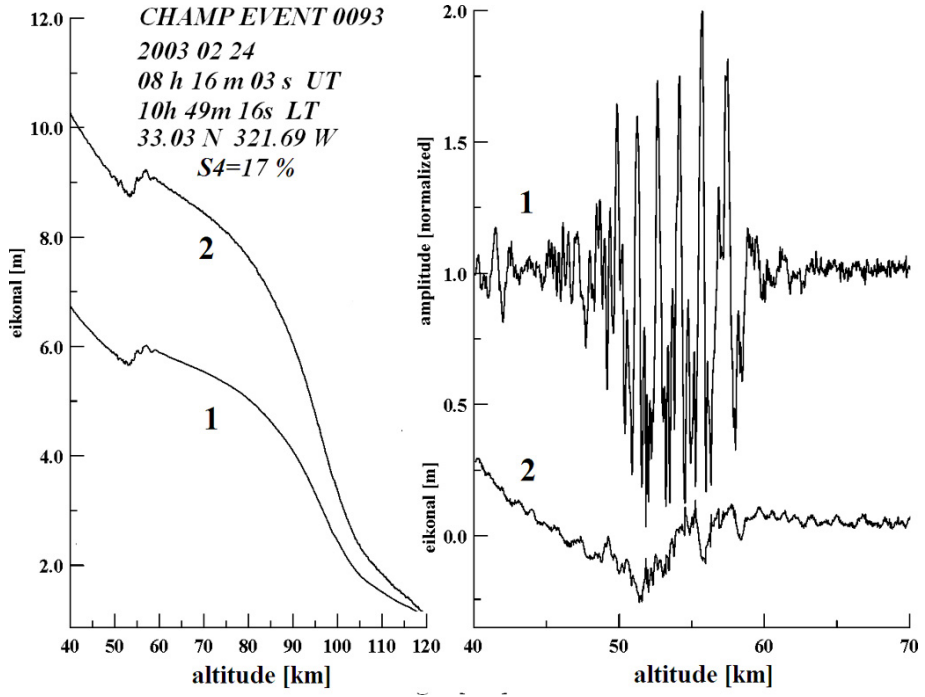

Fig. 3. Quasi-regular variations in the eikonal and amplitude values of the CHAMP RO signals for event No. 0093 (24 February 2003). (left) Eikonal variations at frequencies f_1 and f_2 (curves 1 and 2, respectively). (right) The amplitude (curve 1) and combined eikonal $\Phi(t)$ variations at frequency f_1 (curve 2).

AMTD
4, 1465–1492, 2011

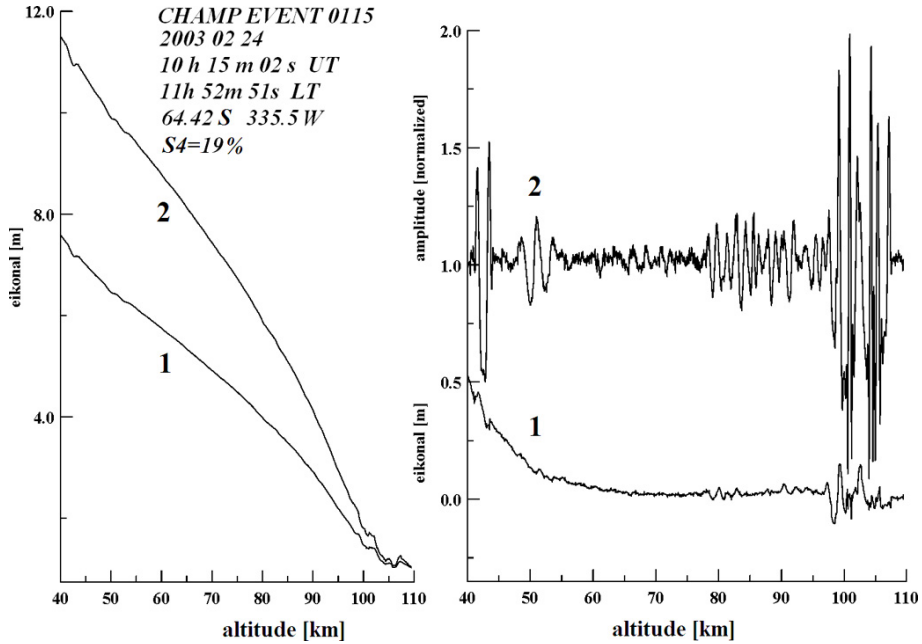

Fig. 4. Amplitude and phase values of the CHAMP RO signals due to diffraction on layered structures of electromagnetic waves in the ionosphere (event No. 0115, 24 February 2003). (left) Eikonal variations at frequencies f_1 and f_2 (curves 1 and 2, respectively). (right) The combined eikonal $\Phi(t)$ (curve 1) and amplitude variations at frequency f_1 (curve 2).

AMTD
4, 1465–1492, 2011

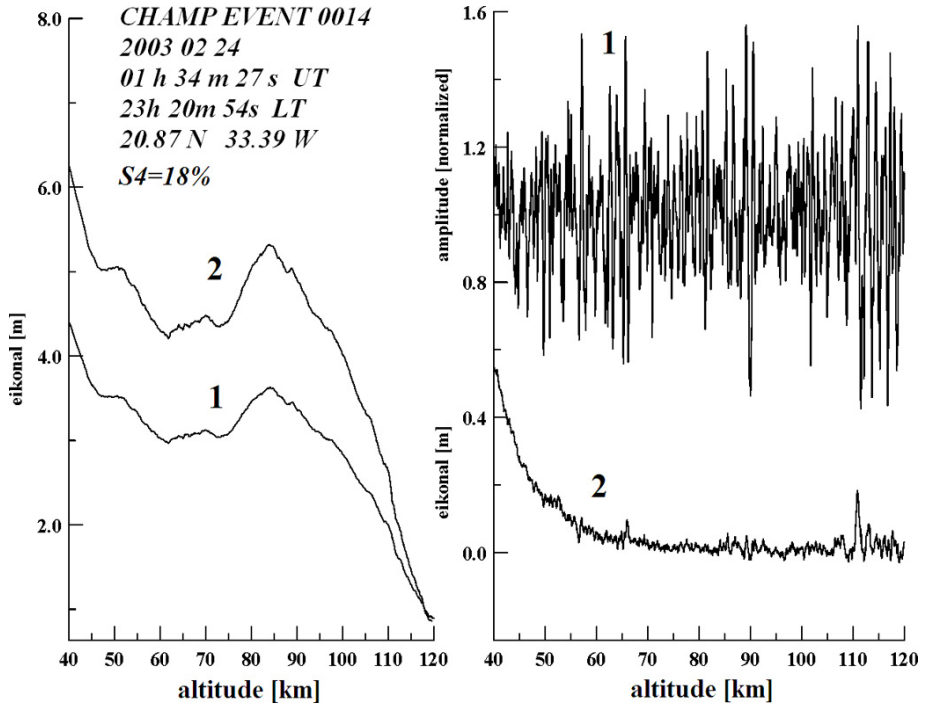

Fig. 5. Amplitude and phase values of the CHAMP RO signal for noisy events No. 0014, 24 February 2003 near geomagnetic equator at local night. (left) Eikonal variations at frequencies f_1 and f_2 (curves 1 and 2, respectively). (right) Amplitude variations at frequency f_1 (curve 1) and the combined eikonal $\Phi(t)$ (curve 2).

AMTD
4, 1465–1492, 2011

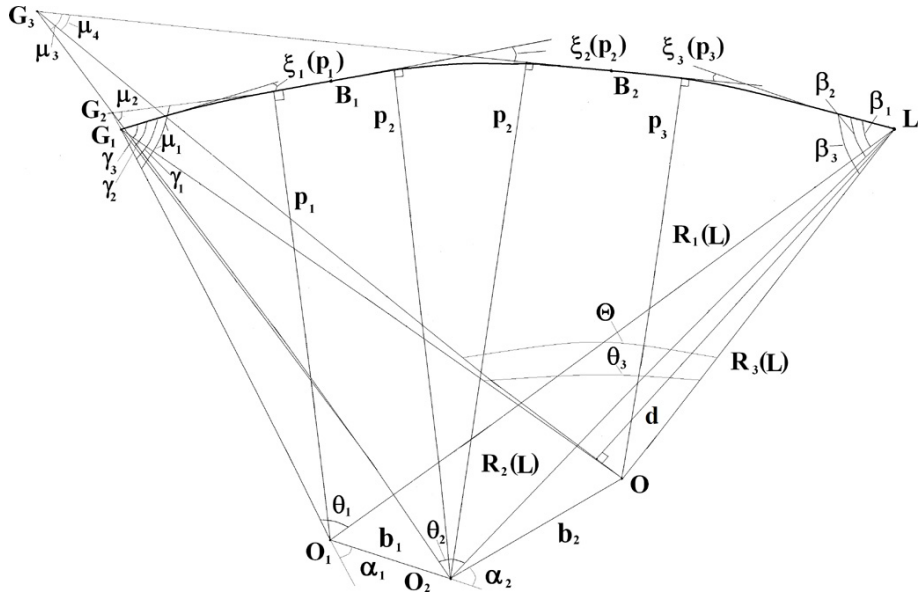

Fig. 6. Geometry of electromagnetic waves propagation through three spherical symmetric sectors. Points G_1, B_1, B_2, L are supposed to be located in the same plane with the centers of spherical symmetry O_1, O_2, and O_3. Points G_2 and G_3 are intersections of the tangents to the ray trajectory $G_1B_1B_2L$ at the points B_1 and B_2 with the straight lines O_1G_1 and O_2G_2, respectively. The angle Θ has vertex at point O_3. The value Θ determines the angle between directions O_3G_3, and O_3L.

AMTD
4, 1465–1492, 2011

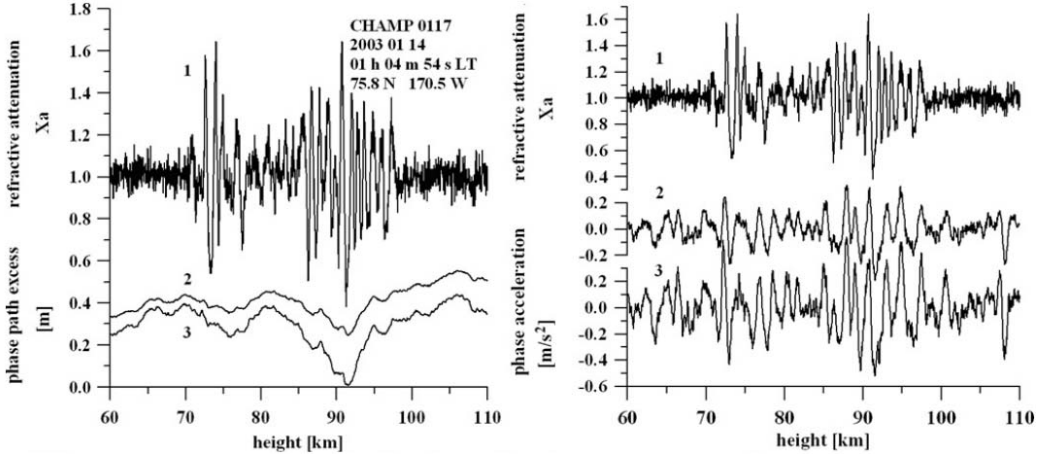

Fig. 7. (left) Refractive attenuation at the first GPS frequency f_1 (curve 1) and the phase path excesses at the frequencies f_1 and f_2 (curves 2 and 3). (right) Comparison of the refractive attenuation at the first GPS frequency f_1 (curve 1) and the eikonal accelerations at the frequencies f_1 and f_2 (curves 2 and 3).

AMTD
4, 1465–1492, 2011

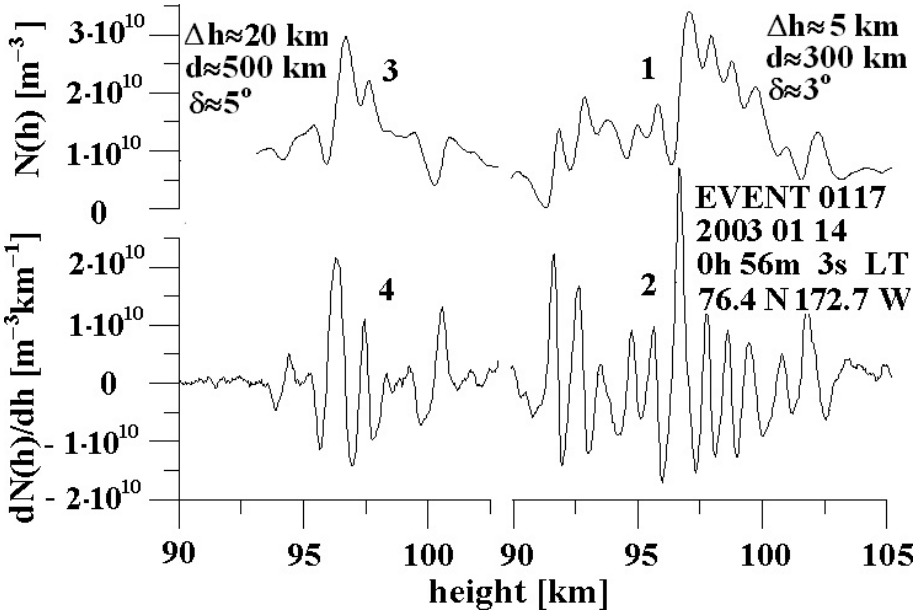

Fig. 8. Vertical distribution of the electron density and its gradient in the main parts of two patches of sporadic E-layer. Curves 1 and 3 describe the electron density distribution, curve 2 and 4 describe the vertical gradient of the electron density.

AMTD
4, 1465–1492, 2011